SUPPORTING MATERIAL

The molecular mechanism by which PIP_2 opens the intracellular G-loop gate of a Kir3.1 channel

Xuan-Yu Meng[1,2], Hong-Xing Zhang[2], Diomedes E. Logothetis[1,*], and Meng Cui[1,*]

[1]Department of Physiology and Biophysics, Virginia Commonwealth University School of Medicine, Richmond, VA 23298, USA
[2]State Key Laboratory of Theoretical and Computational Chemistry, Institute of Theoretical Chemistry, Jilin University, Changchun, 130023, China

[*]correspondence: delogothetis@vcu.edu or mcui@vcu.edu

SUPPLEMENTARY METHODS

Model refinement

Modeller v9.5 (1) was used to build the missing residues as well as side chains in the crystal structures of the Kir3.1 chimera (PDB entry: 2QKS). The constricted conformation of Kir3.1 chimera is missing the C-linker region (ranging from P187 to E192, numbering refers to human Kir3.1 residues), which was resolved in the dilated conformation. Thus the C-linker of the constricted conformation was modeled using the dilated conformation as a template. Additionally, the N-terminus in the dilated (from L60 to R66) and the constricted forms (from Q56 to S69) were also missing and were modeled. Several models were generated by Modeller for two conformations and selected based on internal criteria within the program. The models were then subjected to energy minimization using the CHARMM program with implicit membrane/solvent Generalized Born (GB) model (2) for 1000 steps of a steepest descent minimization.

Molecular docking

An automatic molecular docking program, AUTODOCK (3) was used for the docking studies. Since the size of PIP_2 molecule is too large for flexible docking studies, we replaced it with an analog (diC1), which replaces the two large tails of PIP_2 by two methyl groups. The partial charges of the PIP_2 head group were adopted from the work by Lupyan and colleagues (4). A grid map was generated for the dilated conformation of Kir3.1 chimera using CHNOP (i.e. carbon, hydrogen, nitrogen, oxygen, and phosphor) elements sampled on a uniform grid containing 120×120×120 points, 0.375 Å apart. The center of the grid box was set to the center of known residues critical for PIP_2 sensitivity, i.e. R52, R66, K188, K189, R190, R219, R229, and R313. The Lamarckian Genetic Algorithm (LGA) was selected to identify the binding conformations of the ligands. 100 docking simulations were performed for each of the ligands. The final docked diC1 configurations were selected based on docked binding energies and cluster analysis (see Fig. S4 for the final docked diC1-Kir3.1 chimera that was used for the MD simulations.).

The PIP_2-Kir3.1 chimera complex was constructed based on the docked diC1-Kir3.1 chimera complex structure by superposition and linking of the acyl chains to the docked diC1. The complex structure of PIP_2-Kir3.1 chimera (dilated conformation) was then refined by CHARMM using the same protocol as described in the section of Model refinement. The complex of PIP_2 with constricted conformation was obtained by superposition with the PIP_2-dilated conformation and was also refined by the CHARMM program. The complexes of PIP_2-Kir3.1 chimera (dilated and constricted conformations) were used for molecular dynamics (MD) simulations.

Molecular dynamics (MD) simulations

An explicit lipid bilayer was used to mimic the real membrane environment in MD simulations. The complex of PIP_2-Kir3.1 chimera was immersed in palmitoyloleoyl-phosphatidylcholine (POPC) bilayer generated from the VMD membrane package (5). After being solvated with SPC water molecules, neutralized by Na^+ as the counter ions and including the K^+ ions located in the selectivity filter as obtained from the crystal structures, each system involved ~ 141,000 atoms in the MD simulations. GROMACS

v4.0.5 (6) was used to conduct the simulation with the GROMOS96 53a6 force field (7). The parameters for PIP_2 were generated from the Prodrg server (8). The lipid parameters were obtained from Tieleman through his website (http://moose.bio.ucalgary.ca). Long range electrostatics were calculated using the particle mesh Ewald (PME) method (9) with a 12 Å cut-off. Van der Waal interactions were modeled using Lennard-Jones 6-12 potentials with a 14 Å cut-off. All simulations were conducted at a constant temperature of 300K using the Berendsen thermostat. The system pressure was coupled at isotropic (X+Y, Z) directions referenced to 1 bar using the Berendsen method (10). All bonds were constrained with the LINCS algorithm (11). The time step was 2 fs and the neighboring list was updated every 10 time steps.

Prior to production runs, energy minimization of 3000 steps of steepest descent were carried out on each system followed by a 0.5 ns two-step equilibration process. In the first 0.2 ns, channels, K^+ ions and PIP_2 included in the holo systems were position-restrained using a constant force of 1000 kJ/mol/nm^2, allowing lipid and water molecules to move freely. The restraint was weakened to 10 kJ/mol/nm^2 in the following 0.3 ns equilibration. An electrical field of 0.06 V/nm was applied in this step as well as the production run, along the z-axis of the box to maintain the lower potentials in the intracellular side. The treatment of the electrical field has been detailed in ref (12, 13). A 100 ns production run was conducted on each system and coordinates were saved every 10 ps for analysis. VMD was used for visualization.

Analysis of MD runs

Systems were well equilibrated and stabilized after 20 ns simulations according to root mean square deviations (RMSD) of all channel Cα atoms. The 20-100 ns trajectories of each system were involved in combined principal component analysis (PCA) and interaction network analysis.

PCA is used to extract the collective motions of the protein from the MD simulation trajectory. It describes the motions with a set of eigenvector and eigenvalue pairs which are obtained by diagonalizing the covariance matrix of the Cα atomic positional fluctuations (14, 15). PCA can be also applied to compare two systems for a certain protein, for example, a WT and mutant (16), in the apo and holo systems (17). A trajectory is combined from two independent trajectories and subjected to diagonalization. The resulting eigenvectors describe the internal motions from one protein state to the other. Analysis programs within GROMACS were employed to concatenate trajectories and conduct combined PCA (6).

The interactions of hydrogen bonds, salt bridges and hydrophobic contacts, as well as the DSSP analysis were calculated using the Simulaid program (18). The Simulaid outputs for interactions were reorganized with in-house scripts for facility of comparison among the systems.

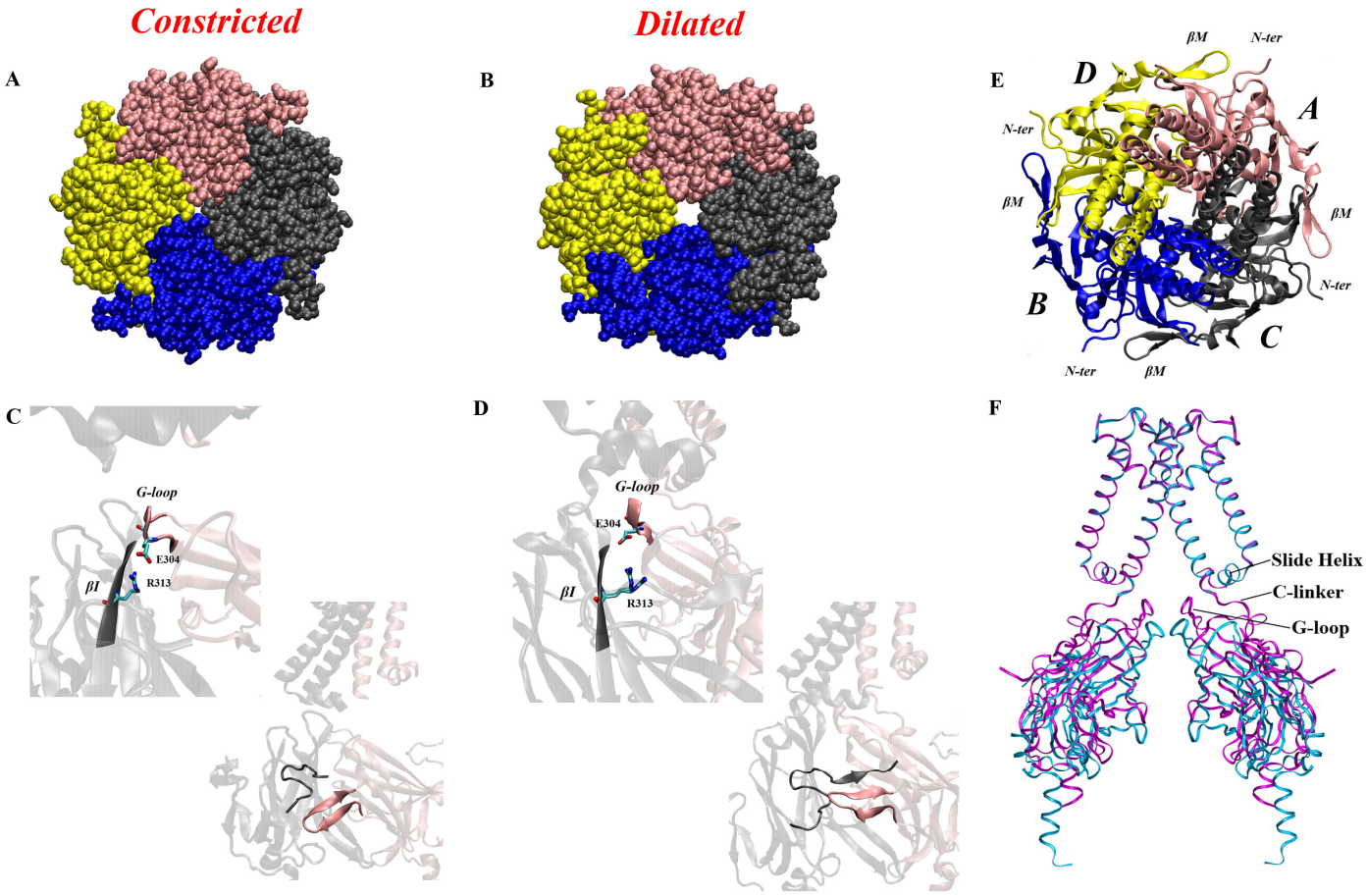

Figure S1. The constricted (latched) and dilated (unlatched) conformations of the Kir3.1 chimera from the crystal structures. (**A**) and (**B**) The cytoplasmic domains of the constricted and dilated forms, respectively. (**C**) and (**D**) Features of the latched interface in the constricted form and unlatched interfaces in the dilated form, respectively. (**E**) Subunit topology, color scheme and cytosolic interfaces used in the study (viewed from extracellular side). (**F**) Superposition of constricted (in red) and dilated (in blue) forms based on the Cα atoms of transmembrane regions. Identification of some critical regions involved in this study.

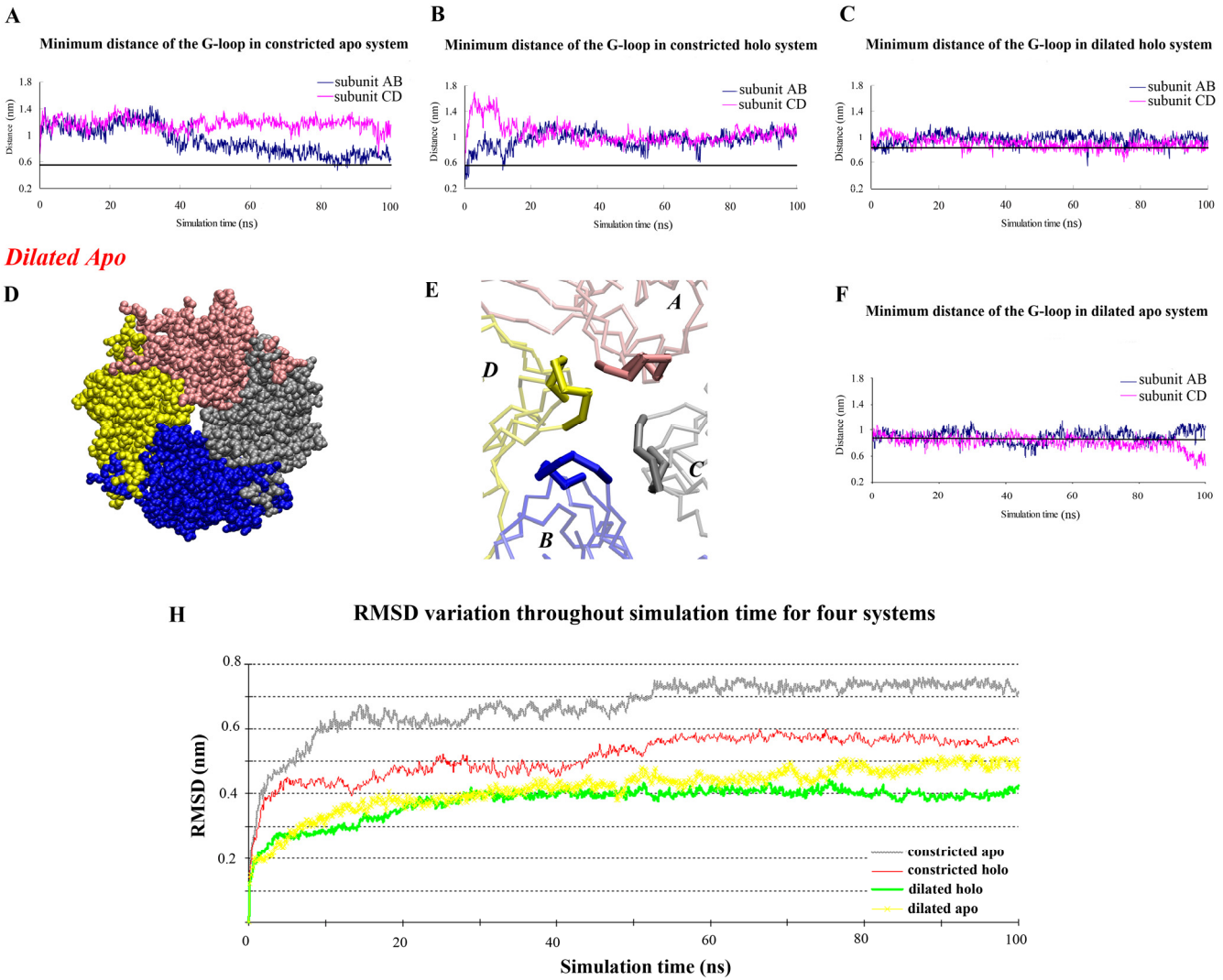

Figure S2. Minimal distances and RMSD analysis in four simulated systems. (**A-C**) and (**F**) Minimal distance variation of the G-loop gates between diagonal subunits through the100 ns simulation time. G-loop residues T305 to T309 were used for minimal distance calculations. The black horizontal lines in each of the panels indicate initial values of the G-loop minimal distances: constricted form ((**A**) and (**B**)) is 0.55nm and dilated form ((**C**) and (**F**)) is 0.82nm (19). (**D**) The cytoplasmic domain of dilated apo system at the end of the simulation viewed from the extracellular side. The transmembrane domain was removed to display the G-loop gate; (**E**) The Cα trace of the G-loop gates from each of the four subunits A-D corresponding to panel (**D**). (**H**) RMSD variations for each system throughout the simulation. RMSDs were calculated based on all the Cα atoms of the channel.

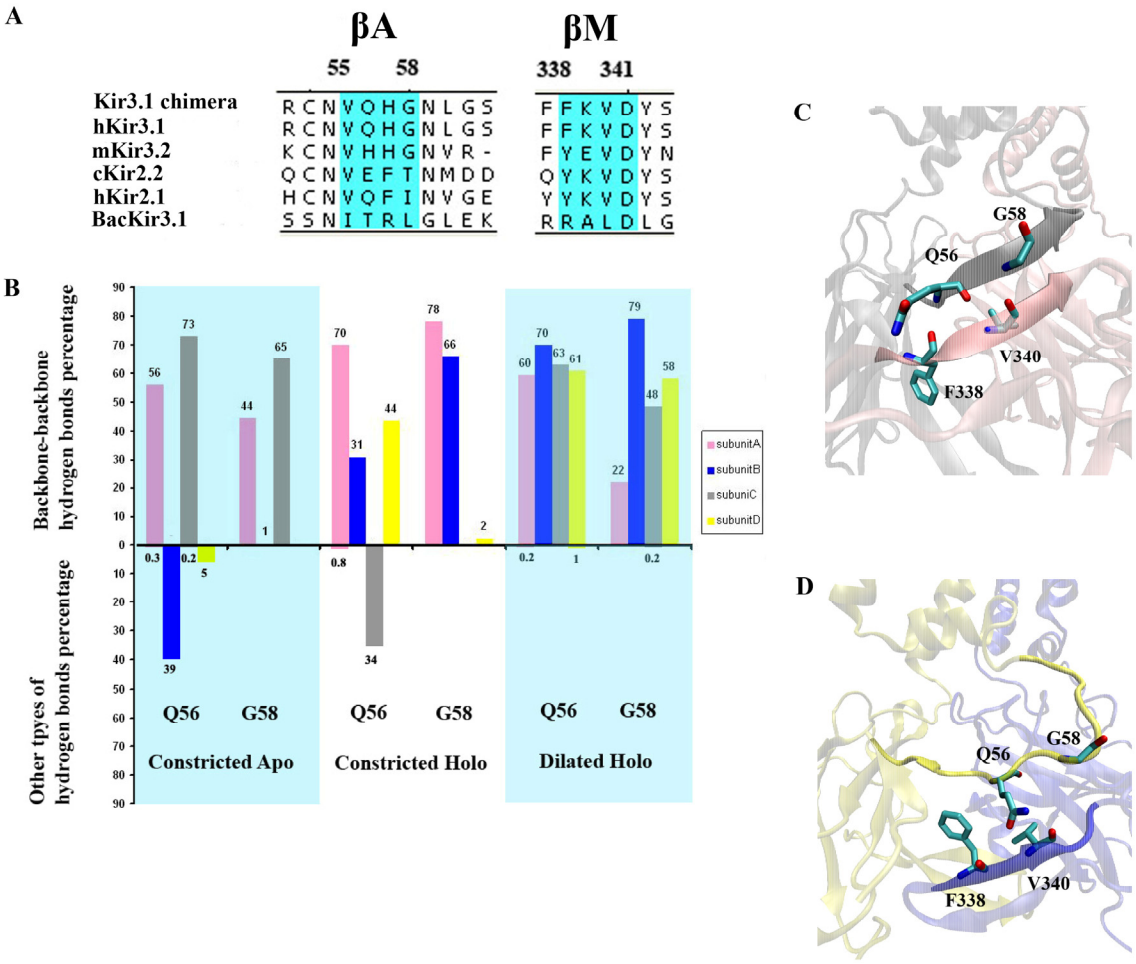

Figure S3. **Statistics of intersubunit hydrogen bond formation between the βA of the N-terminus and the βM of the C-terminus throughout the simulation time.** (**A**) Sequence alignment among several Kir channels with highlighted βA and βM residues. The residue numbers are based on hKir3.1. (**B**)Survival percentage of between the βA and βM was calculated between 20-100 ns of the simulation time for the three systems, involving Q56 and G58 in the βA and F338, V340 and Y342 in the βM. The backbone-backbone hydrogen bonds between Q56-F338/V340 and G58-V340/Y342 indicate the formation of βA/βM sheet (unlatched interface, as shown in (C)); otherwise Q56 tends to form sidechain-backbone hydrogen bonds with the βM residues (latched interface, as shown in (C)). (**C**) and (**D**) were generated using the last snapshot of constricted holo system from MD trajectory, representing interface between subunits AC and subunit BD, respectively. The constricted apo system has Q56/G58 from subunits A and C forming backbone-backbone hydrogen bonds with βM; The constricted holo system shows three subunits A, B and D; and the dilated holo system shows all four subunits forming such hydrogen bonds.

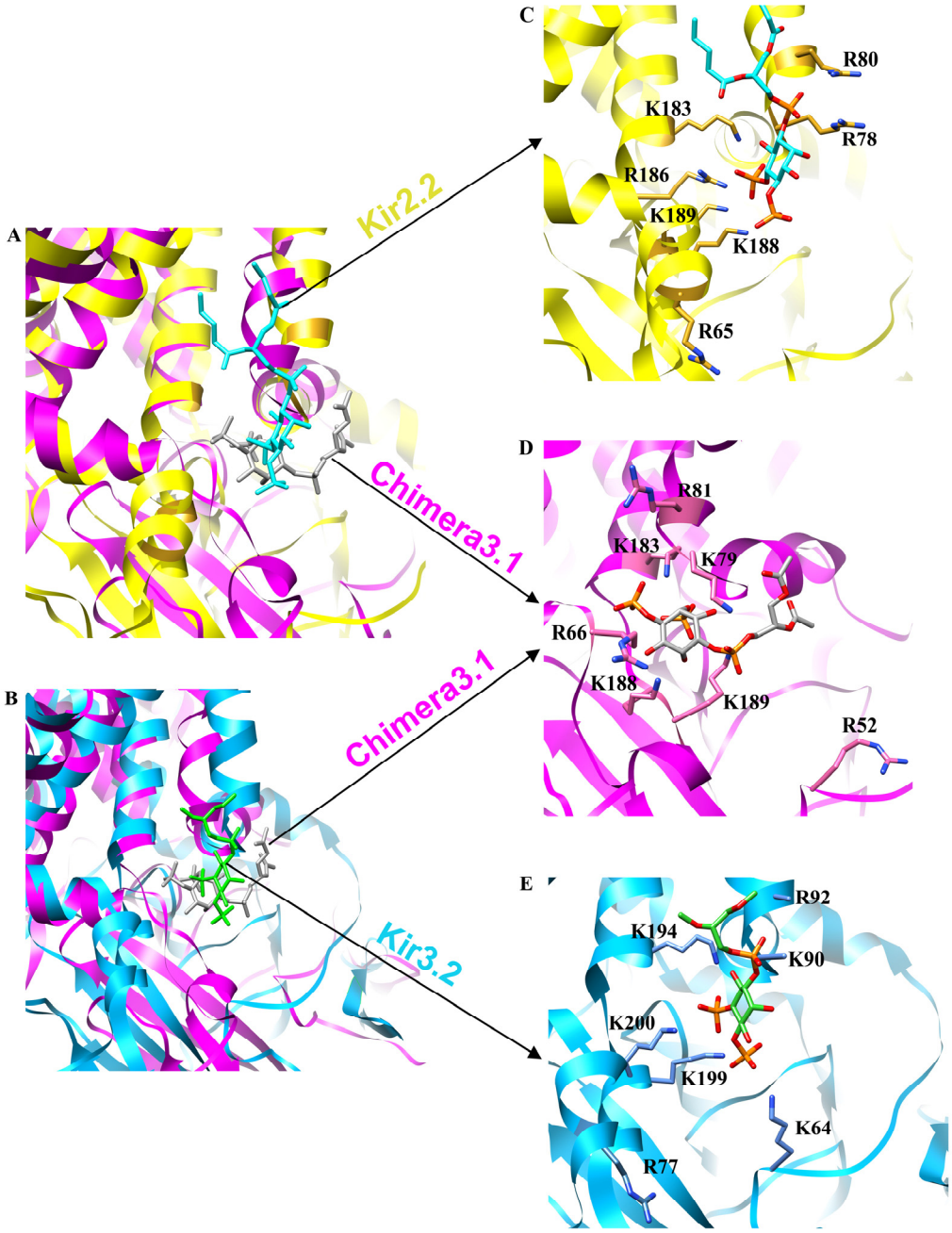

Channel	Residue							
Kir3.1 chimera	**R52**	**R66**	**K79**	**R81**	**K183**	Q186	**K188**	**K189**
Kir2.2	Q51	R65	**R78**	**R80**	**K183**	**R186**	**K188**	**K189**
Kir3.2	**K64**	R77	**K90**	**R92**	**K194**	Q197	**K199**	**K200**

Figure S4. The comparison of PIP_2 binding modes between the docked Kir3.1 chimera model to each of the Kir2.2 (20) and Kir3.2 (21) co-crystal structures, respectively. Residues shown in the (**C**), (**D**) and (**E**) are listed in the Table with homologous residues arranged in each column. Residues shown in bold interact with PIP_2, while those not in bold do not.

The final conformation of the docked PIP_2 onto the channel was selected based on three considerations: 1) PIP_2 should form stable salt bridges with residues that have been

experimentally shown to affect PIP_2 sensitivity, i.e. R52, R66, K188, K189, R190, R219, R229 and R313 (Kir3.1 residue numbering; not all of the residues identified by our model satisfied this consideration, since some, such as R229 and R313, are far away in the 3D structure, thus most likely acting allosterically to affect PIP_2 sensitivity). 2) Since PIP_2 is a signaling lipid molecule located in the membrane, it is likely for PIP_2 to bind into the interface between the transmembrane domain and the cytoplasmic domain. 3) We used diC1 (in analogy to PIP_2) to conduct docking studies, then linked the acyl chains to the docking diC1 and obtained the complex structure of the full PIP_2 binding onto the channel. Thus the pose of diC1 we selected should ensure that the linked tails can insert into the membrane rather than conflict with the channel.

We superimposed the PIP_2-bound Kir3.1 chimera (chimera in magenta and PIP_2 in gray) with PIP_2-Kir2.2 (PDB: 3SPI, Kir2.2 in yellow and PIP_2 in cyan) based on the Slide helix, the transmembrane domains and the C-linker, in order to match the PIP_2 binding regions, as shown in (A). The same superposition was also conducted between Kir3.1 chimera and Kir3.2 (PDB: 3SYA, Kir3.2 in light blue and PIP_2 in green), as shown in (**B**).

(**C**), (**D**) and (**E**) show positively charged residues related to the PIP_2 binding in the Kir2.2, Kir3.1 chimera and Kir3.2, respectively. The PIP_2-chimera structure used here is the docked model prior to the MD simulations (see Materials and Methods/Molecular docking).

As shown in (**A**) and (**B**), the PIP_2 binding region in our predicted model is in close agreement with the interacting regions seen in the crystal structures. Residues forming salt-bridge interactions with PIP_2 in our model are R66, K79, R81, K183, K188 and K189. The major interactions, i.e. K79, R81, K183, K188 and K189, are also found in the crystal structures of PIP_2-Kir2.2 and PIP_2-Kir3.2. R66 does not interact with PIP_2 in either Kir2.2 or Kir3.2 due to a bending of the Slide Helix. This bending of the Slide Helix leads to a conformational change that positions R66 away from the PIP_2 binding region.

Significant differences in salt-bridge interactions also exist between the Kir2.2 and Kir3.2 structures. The N-terminal residue K64 that contacts PIP_2 in Kir3.2 corresponds to Q51 in Kir2.2, which does not interact with PIP_2. Just as in Kir3.2, the corresponding R52 residue in our model of the Kir3.1 chimera formed stable salt bridge with PIP_2 in the MD simulations (constricted holo). R186 in Kir2.2 is involved in PIP_2 binding; this residue corresponds to Q186 in Kir3.1 chimera and Q197 in Kir3.2, neither of which interact with PIP_2.

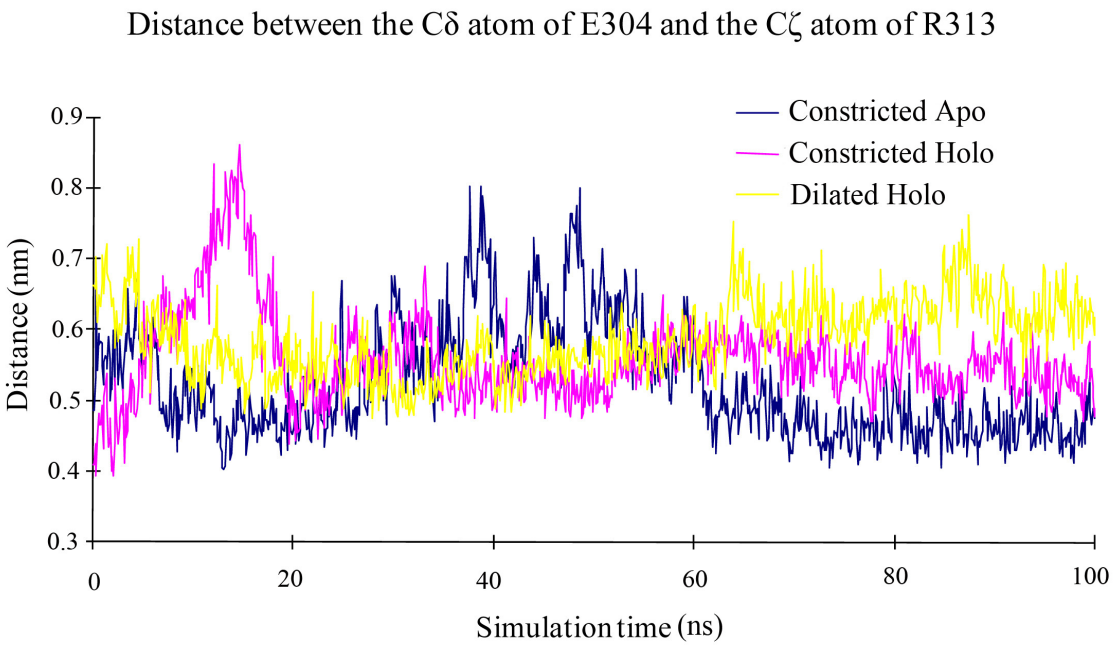

Figure S5. Distance between the Cδ atom of E304 and the Cζ atom of R313 of the salt bridge E304-R313 in the apo and holo constricted, and holo dilated systems during the MD simulations. The E304-R313 distance (the average among the four subunits) was monitored during the 100ns simulation time for the three systems. The distance increase from the constricted apo system to the dilated holo system indicates that E304-R313 stabilizes the closed state of the G-loop gate and weakening of this interaction is required to open the gate.

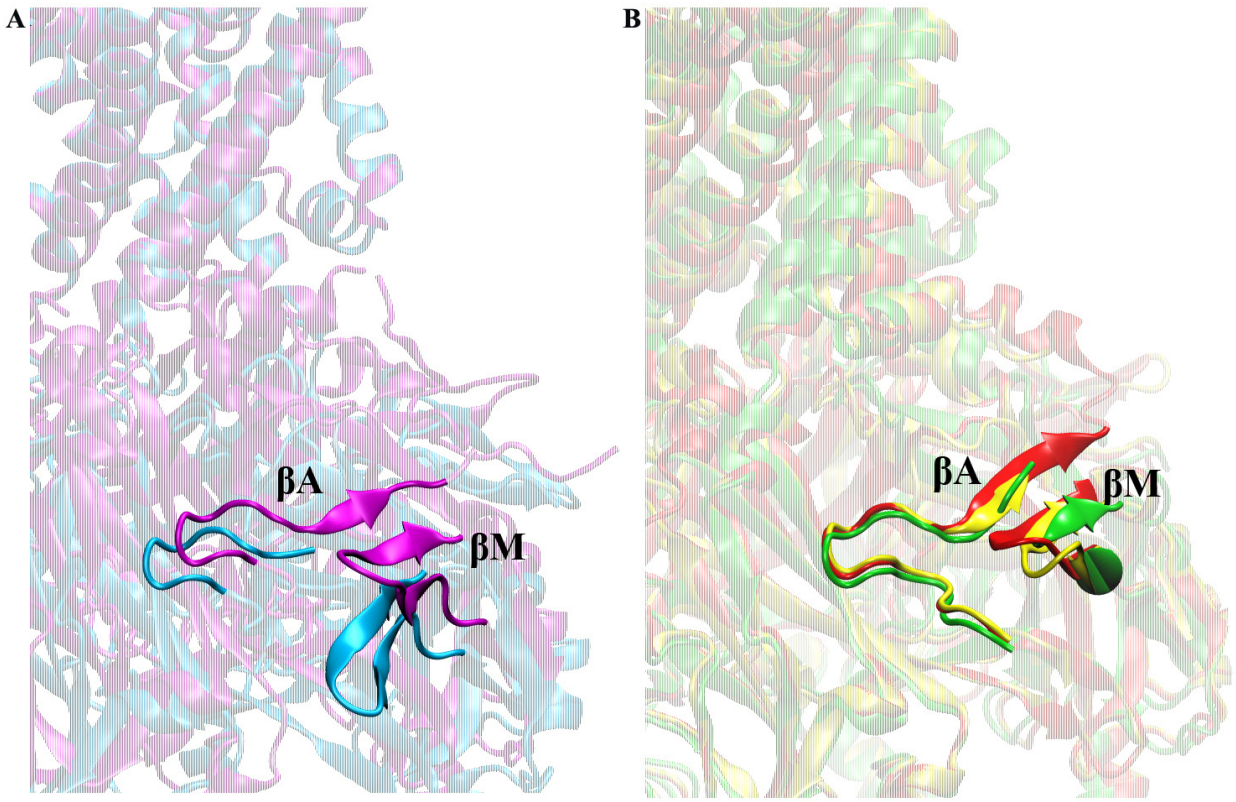

Figure S6. The intersubunit interaction of βA and βM in Kir3.1 chimera (**A**) and Kir3.2 (**B**) crystal structures reveals distinct gating movements.

In the Kir3.1 chimera (**A**), the βM moves upward and forms a stable interaction with the βA when the G-loop transitions from the closed (in cyan) to the open (in magenta) conformation. A similar phenomenon is found in the KirBac3.1 crystal structures (22).

As shown in (B), we superimposed the cytoplasmic domains of Kir3.2 crystal structures (21) 3SYA (closed G-loop gate, in red), 3SYP (open G-loop gate, in yellow) and a completely open model constructed based on 3SYQ (both G-loop and helix bundle crossing gates are open, in green). The opening of the G-loop gate occurs simultaneously with the outward movement of the LM-loop. The βA also shows a slight displacement together with the βM.

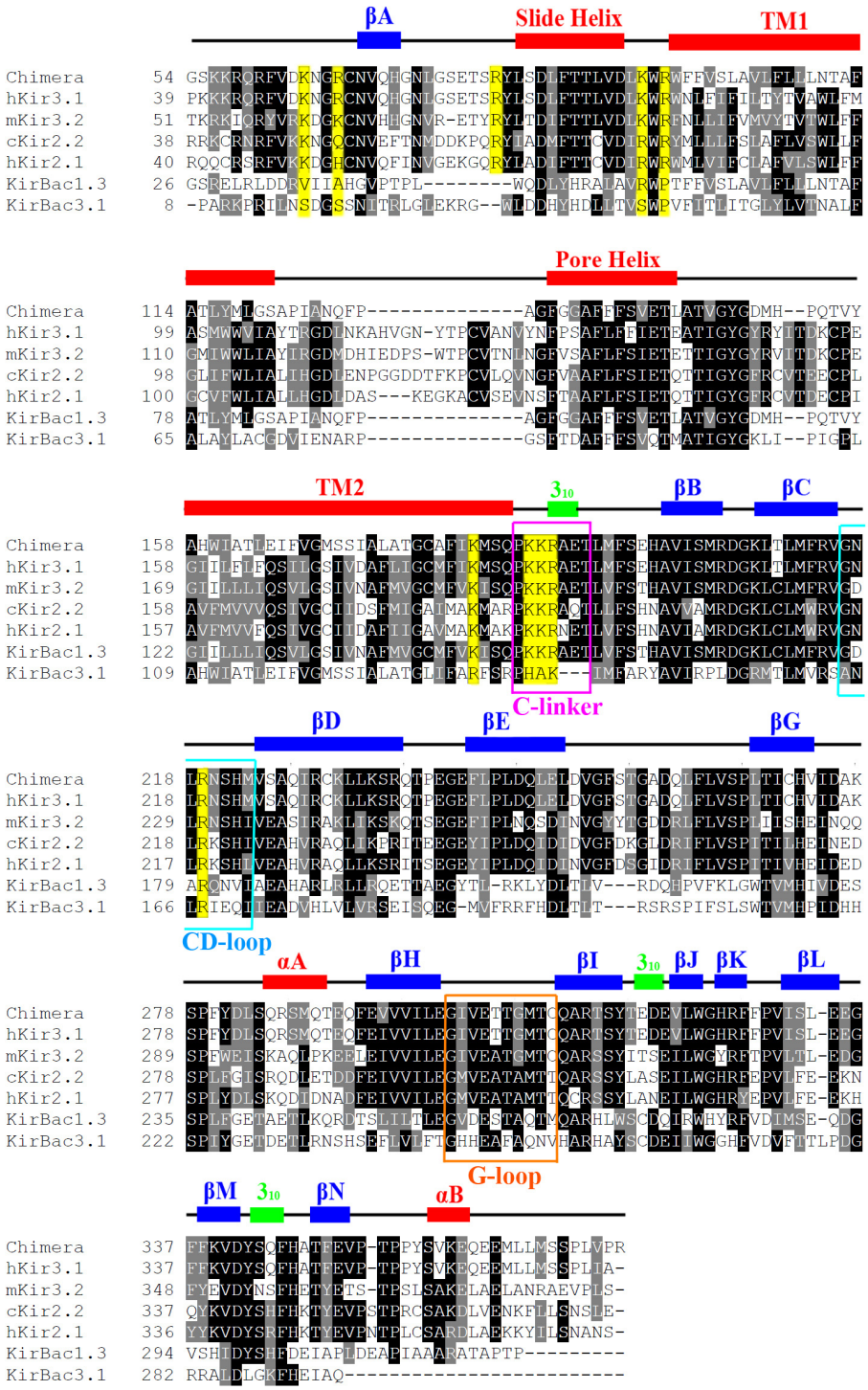

Figure S7. Multiple sequence alignment and secondary structural elements. Black background indicates residue identity and gray residue conservation. Residues forming salt bridges with PIP_2 in the MD simulations are highlighted in yellow. The secondary structure nomenclature adopted is from MacKinnon's assignments for the Kir3.1 chimera (19). The residue numbering for the Kir3.1 chimera [a chimera between the mouse Kir3.1 (K41-W81, I182-L371) and the bacterial KirBac1.3 (F62-F145)] is identical to the hKir3.1 shown (23). The hKir3.1 and mKir3.1 show 4 amino acid differences in the sequences shown: hKir3.1m (I295V, T396S, A481P, A481T).

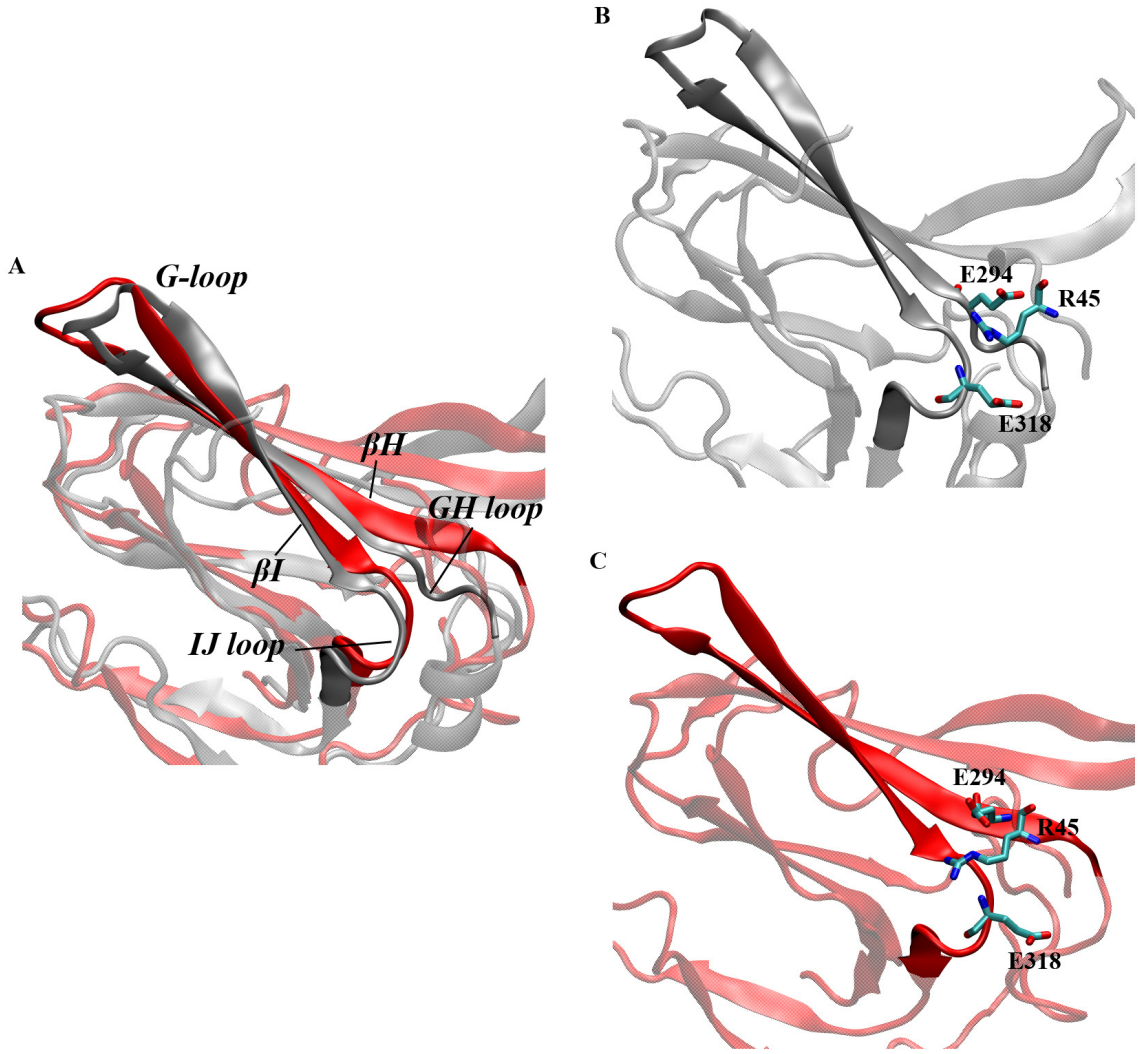

Figure S8. **A PIP_2-driven N-terminal switch between the GH and IJ loops**. (**A**) Superposition of cytoplasmic domains of subunit D for constricted apo (grey) and constricted holo (red) based on Cα atoms. The βH and βI strands cross to harbor the G-loop on one end, and the IJ and GH loop on the other. (**B**) In the constricted apo structure, the N-terminal R45 forms a salt bridge with E318 of the IJ loop. (**C**) In the constricted holo form, R45 switches to mainly interact with E294 in the GH loop. As can be seen in the superimposed structures (A) this switching of interactions is accompanied by a change in the conformation of the G-loop gate.

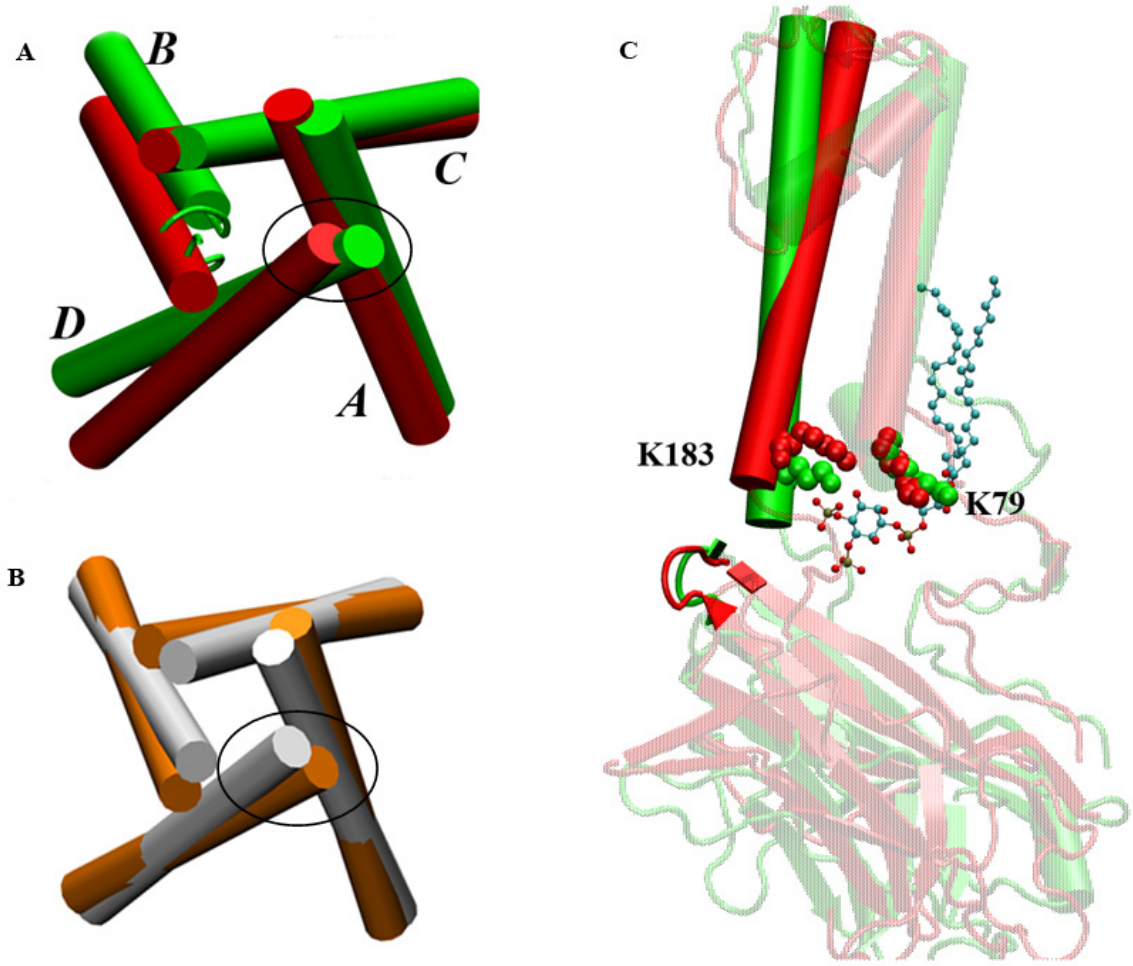

Figure S9. The beginnings of the PIP_2-driven change in the inner helix gate. (**A**) TM2 of the constricted holo (green) and dilated holo (red) structures viewed from the intracellular side. Superposition was generated based on Cα atoms of the cytoplasmic domains of the constricted holo and dilated holo structures of the Kir3.1 chimera. (**B**) Superposition of KcsA closed (white, PDB: 1K4C) (24) and open (orange, PDB: 3FB8) (Cuello et.al., 2008, to be published) structures based on the Cα atoms for comparison. (**C**) Superposition of constricted holo (green) and dilated holo (red) based on the TM1 Cα atoms of subunit D.

Table S1. Percentage of residue hydrogen-bond interactions (unless otherwise indicated) formed during 20-100ns simulation time (related to Fig 4-6)

				Constricted Apo								Constricted Holo								Dilated Holo							
				A	B	C	D	AC	BC	BD	AD	A	B	C	D	AC	BC	BD	AD	A	B	C	D	AC	BC	BD	AD
R	45	E	294 stb	7	6	39	4					66	15	21	26					21	56	35	6				
R	45	E	318 stb	19		5	47					2		1	1							3					
Q	56	F	338					73 BB	39 SB		32 BB					35 SB			70\1 BB\SB					63 BB	70 BB	61\1 BB\SB	60 BB
Q	56	V	340					71 BB	1 SB	5 SB	56 BB					7 SB	31 BB	44 BB	53 BB					63 BB	53 BB	60 BB	50 BB
G	58	V	340					65 BB	1 BB		44 BB						66 BB		78 BB					48 BB	79 BB	57 BB	22 BB
G	58	Y	342															2 BB						7 BB	37 BB	58 BB	
R	66	R	219					18 SB	6 SB		25 SB																
R	66	N	220					5 SS	1 SS	14 SB	1 SS						1\3 SS\SB										
R	66	S	221														26 SS										
K	183	V	76	15 SB	24 SB	23 SB	13 SB					13 SB	13 SB	12 SB	32 SB					33 SB	1 SB	26 SB	11 SB				
K	183	L	78	25 SB	21 SB	30 SB	28 SB					27 SB	23 SB	35 SB	13 SB					10 SB	10 SB	16 SB	8 SB				
R	190	K	49		7 SB									4 SB	3 SB					8 SB	35 SB	1 SB					
R	190	N	50	1\1 SS\SB	1\2 SS\SB	7\9 SB\SS	25\5 SB\SS						3\4 SB\BS	9 SS						2\11 SS\SB	1\9 SS\BS	1\13 SB\SS	6\12\3 SB\BS\SS				
R	190	R	313		10 SB									3 SB						23 SB	1 SB	11 SB					
R	190	T	314											2 SS						8 SS	11 SS	27 SS					
R	219	C	53					3 SB		3 SB	22\2 SS\SB					1 SB	10 SB		4 SS								
R	219	V	55							10 SB	1 SB					7 SB			1 SB								
R	219	H	57					2 SS	19 SS	15\15 SS\BS	18 SS					3 SS	8 SS	1 SS	3 SS								
H	222	E	304	15\6 BB\SS	6\44 SS\BB	54\13 BB\SS	6\56 SS\BB					9\18 BB\SS	39 BB	1 SS	21\59 SS\BB					34\20\35 SS\BS\BB	47\40\34 SS\BS\BB	59\24\48 SS\BS\BB	50\47\25 BS\SS\BB				
V	224	C	53 hp					16	23	33	3					32	31										
V	224	I	302										23 BB							70 BB	67 BB	59 BB	67 BB				
S	225	E	300															39 SS						70\27 SS\BS	13\55 BS\SS	64\22 SS\BS	74\43 SS\BS
S	225	I	302	45 BB	5 BB	12 BB	10 BB					22 BB	9 BB	29 BB	9 BB							3 BB					
E	304	C	53													5\11 SB\SS	1 SS										
R	313	D	48											27 SB	7 SB								29 SB				
R	313	K	49											1 SB	8\2 BS\SB								1\2\10 BS\BB\SB				
R	313	G	51	1 BB		19\33 BB\SB	2\8 SB\BB					1 SB	23 SB	11 SB						45 SB	32 SB	29 SB	15 SB				
R	313	E	304 stb					49	33	40	63					30	71	14	36					14	34	23	47

Note: stb: salt-bridge; hp: hydrophobic; BB: backbone-backbone; SB: sidechain-backbone; BS: backbone-sidechain; SS: sidechain-sidechain.

SUPPLEMENTARY REFERENCES

1. Sali, A., L. Potterton, F. Yuan, H. van Vlijmen, and M. Karplus. 1995. Evaluation of comparative protein modeling by MODELLER. Proteins 23:318-326.
2. Im, W., M. S. Lee, and C. L. Brooks, 3rd. 2003. Generalized born model with a simple smoothing function. J Comput Chem 24:1691-1702.
3. Morris, G. M., D. S. Goodsell, R. S. Halliday, R. Huey, W. E. Hart, R. K. Belew, and A. J. Olson. 1998. Automated docking using a Lamarckian genetic algorithm and an empirical binding free energy function. Journal of Computational Chemistry 19:1639-1662.
4. Lupyan, D., M. Mezei, D. E. Logothetis, and R. Osman. 2010. A molecular dynamics investigation of lipid bilayer perturbation by PIP2. Biophys J 98:240-247.
5. Humphrey, W., A. Dalke, and K. Schulten. 1996. VMD: Visual molecular dynamics. Journal of Molecular Graphics 14:33-&.
6. Hess, B., C. Kutzner, D. van der Spoel, and E. Lindahl. 2008. GROMACS 4: Algorithms for highly efficient, load-balanced, and scalable molecular simulation. Journal of Chemical Theory and Computation 4:435-447.
7. Oostenbrink, C., A. Villa, A. E. Mark, and W. F. Van Gunsteren. 2004. A biomolecular force field based on the free enthalpy of hydration and solvation: The GROMOS force-field parameter sets 53A5 and 53A6. Journal of Computational Chemistry 25:1656-1676.
8. Schuttelkopf, A. W., and D. M. F. van Aalten. 2004. PRODRG: a tool for high-throughput crystallography of protein-ligand complexes. Acta Crystallographica Section D-Biological Crystallography 60:1355-1363.
9. Darden, T., D. York, and L. Pedersen. 1993. Particle Mesh Ewald - an N.Log(N) Method for Ewald Sums in Large Systems. Journal of Chemical Physics 98:10089-10092.
10. Berendsen, H. J. C., J. P. M. Postma, W. F. Vangunsteren, A. Dinola, and J. R. Haak. 1984. Molecular-Dynamics with Coupling to an External Bath. Journal of Chemical Physics 81:3684-3690.
11. Hess, B., H. Bekker, H. J. C. Berendsen, and J. G. E. M. Fraaije. 1997. LINCS: A linear constraint solver for molecular simulations. Journal of Computational Chemistry 18:1463-1472.
12. Roux, B. 2008. The Membrane Potential and its Representation by a Constant Electric Field in Computer Simulations. Biophysical Journal 95:4205-4216.
13. Bjelkmar, P., P. S. Niemela, I. Vattulainen, and E. Lindahl. 2009. Conformational Changes and Slow Dynamics through Microsecond Polarized Atomistic Molecular Simulation of an Integral Kv1.2 Ion Channel. Plos Computational Biology 5.
14. Amadei, A., A. B. M. Linssen, and H. J. C. Berendsen. 1993. Essential Dynamics of Proteins. Proteins-Structure Function and Genetics 17:412-425.
15. Amadei, A., M. A. Ceruso, and A. Di Nola. 1999. On the convergence of the conformational coordinates basis set obtained by the essential dynamics analysis of proteins' molecular dynamics simulations. Proteins-Structure Function and Genetics 36:419-424.
16. Ceruso, M. A., A. Grottesi, and A. Di Nola. 2003. Dynamic effects of mutations within two loops of cytochrome c(551) from Pseudomonas aeruginosa. Proteins-Structure Function and Genetics 50:222-229.
17. van Aalten, D. M. F., J. B. C. Findlay, A. Amadei, and H. J. C. Berendsen. 1995. Essential dynamics of the cellular retinol-binding protein - Evidence for ligand-induced conformational changes. Protein Engineering 8:1129-1135.
18. Mezei, M. 2010. Simulaid: A Simulation Facilitator and Analysis Program. Journal of Computational Chemistry 31:2658-2668.
19. Nishida, M., M. Cadene, B. T. Chait, and R. MacKinnon. 2007. Crystal structure of a Kir3.1-prokaryotic Kir channel chimera. Embo Journal 26:4005-4015.

20. Hansen, S. B., X. Tao, and R. MacKinnon. 2011. Structural basis of PIP2 activation of the classical inward rectifier K+ channel Kir2.2. Nature 477:495-498.
21. Whorton, MatthewÂ R., and R. MacKinnon. 2011. Crystal Structure of the Mammalian GIRK2 K+ Channel and Gating Regulation by G Proteins, PIP2, and Sodium. Cell 147:199-208.
22. Clarke, O. B., A. T. Caputo, A. P. Hill, J. I. Vandenberg, B. J. Smith, and J. M. Gulbis. 2010. Domain Reorientation and Rotation of an Intracellular Assembly Regulate Conduction in Kir Potassium Channels. Cell 141:1018-1029.
23. Chan, K. W., M. N. Langan, J. L. Sui, J. A. Kozak, A. Pabon, J. A. Ladias, and D. E. Logothetis. 1996. A recombinant inwardly rectifying potassium channel coupled to GTP-binding proteins. J Gen Physiol 107:381-397.
24. Zhou, Y., J. H. Morais-Cabral, A. Kaufman, and R. MacKinnon. 2001. Chemistry of ion coordination and hydration revealed by a K+ channel-Fab complex at 2.0 A resolution. Nature 414:43-48.